IEEE Robotics and Automation Letters (RA-L) paper, presented at ICRA 2024, Yokohama, Japan. Cite as RA-L paper.

Design and Control of a Transformable Multi-Mode Mobile Robot

Haoran Li, *Graduate Student Member, IEEE*, Yongzhong Bu, Yongjian Bu, Shixin Mao, Yisheng Guan, and Haifei Zhu, *Member, IEEE*

***Abstract*—Conventional mobile robots typically include a single locomotion mode and require additional arms to transport objects. To address the challenges of traversing in diverse environments and transporting objects, a novel transformable multi-mode Mecanum-wheeled mobile robot is proposed in this paper. Owing to its unique foreleg design, the robot could operate either in the quadrilateral four-wheel mode, collinear four-wheel mode, or upright two-wheel mode; it could even smoothly switch between any two modes by re-arranging the foreleg wheels. When standing with its forelegs raised, the robot can carry objects and transport them to a predetermined destination. The design and operational modes of the robot were explored in detail. The kinematics and control of the different operational modes were analyzed and experimentally verified. The results indicate that the developed robot can perform versatile locomotion to accomplish object transportation in diverse environments by utilizing its foreleg-wheel mechanisms. Furthermore, the robot experiences an additional angular velocity because of an asymmetric arrangement of the front and rear Mecanum wheels, which differs from conventional symmetric arrangements.**

***Index Terms*—Kinematics, motion control, wheeled robots.**

I. Introduction

NUMEROUS mobile robots have been deployed in diverse environments, such as factories, warehouses, hospitals, and offices for different tasks [1]. Object transportation is a frequently used application requiring mobile robots to exhibit adequate trafficability and a good ability to carry objects.

Leg-wheel hybrid locomotion is a promising means of ensuring suitable maneuverability and trafficability of mobile robots, particularly when omnidirectional wheels are used. Recently developed representatives include an omnidirectional mobile robot (OMR) with an active suspension [2], a Mecanum-wheeled hybrid hexapod robot [3], and an OMR with ground reaction force-compensated wheel-leg mechanisms [4]. These leg-wheel hybrid mobile robots exhibit appropriate adaptability in heterogeneous scenarios and irregular terrains owing to their wheeled, legged, or hybrid locomotion modes. Another common and effective method for achieving adequate maneuverability and trafficability is employing variable locomotion configurations. For instance, the AZIMUT robot used leg-track-wheel articulations [5], the OmniWheg robot was configured with separable omnidirectional wheels [6], and the MIRRAX robot comprised a reconfigurable body for varying the Mecanum wheel arrangements [7]. However, these mobile robots cannot transport objects without additional mechanisms.

The addition of dedicated arms to carry objects enables object-transportation functions in different types of mobile robots, including the OMR with a PA-10 arm [8], and the Boston Spot with an external robotic arm [9]. Humanoid robots designed with a track-leg or wheel-leg chassis, such as CHIMP [10], JUSTIN [11], and CENTAURO [12], can perform dual-arm transportation missions in diverse environments. However, this introduces highly redundant robotic systems, resulting in complex systems and controls. Particularly, when the support polygon of a composite robot system is a variable, the planning and control of the arm under balanced constraints are challenging.

The methods by which legged robots manipulate objects have been categorized into four classes [13]: object interactions without grasping, manipulation with walking legs, dedicated non-locomotive arms, and legged teams. The integrated mechanisms of mobile robots, such as walking legs, can be advantageous to carry and move objects. For instance, several methods have been proposed for hexapod robots that carry objects by transforming one or two legs into arms while walking on the remaining legs [14]. A novel integrated modular neural control approach was implemented in a dung beetle-like robot to achieve versatile locomotion and object transportation on flat and uneven terrains [15]. Additionally, leg-wheel quadrupedal robots have the potential to complete some tasks by raising their two forelegs [16]. However, to enable quadruped robots raise their forelegs to transport objects, further studies on the motion planning and control are required due to fundamental changes in the locomotion paradigm and balance state.

Inspired by the ideas of varying locomotion configurations and utilizing integrated leg-wheel mechanisms, a novel transformable multi-mode Mecanum-wheel-driven mobile robot is proposed in this study (Fig. 1). The robot was designed using four Mecanum wheels, two of which were linked to the chassis using active parallelogram linkage mechanisms (forelegs). This

Manuscript received 8 July 2023; accepted 26 November 2023. Date of publication 18 December 2023; date of current version 28 December 2023. This letter was recommended for publication by Associate Editor S. Jeon and Editor C. Gosselin upon evaluation of the reviewers' comments. This work was supported in part by the Science and Technology Plan of Guangdong Province—Guangdong-Hong Kong-Macao Joint Innovation Project under Grant 2023A0505010016, in part by the Research and Development Programs in Key Areas of Guangdong Province under Grant 2020B090928002, in part by the Basic and Applied Basic Research Fund of Guangdong Province Project under Grant 2022A1515240013, and in part by the Foshan Science and Technology Innovation Team Project under Grant FS0AA-KJ919-4402-0098. *(Corresponding author: Haifei Zhu.)*

Haoran Li, Yongzhong Bu, Yongjian Bu, Yisheng Guan, and Haifei Zhu are with the School of Electromechanical Engineering, Guangdong University of Technology, Guangzhou 510006, China (e-mail: 610216623@qq.com; 3216932538@qq.com; 1923946334@qq.com; ysguan@gdut.edu.cn; hfzhu@gdut.edu.cn).

Shixin Mao is with Jiutian Innovation (Guangdong) Intelligent Technology Co., Ltd, Foshan 528299, China (e-mail: maosx@mail.ustc.edu.cn).

This letter has supplementary downloadable material available at https://doi.org/10.1109/LRA.2023.3344352, provided by the authors.

Digital Object Identifier 10.1109/LRA.2023.3344352

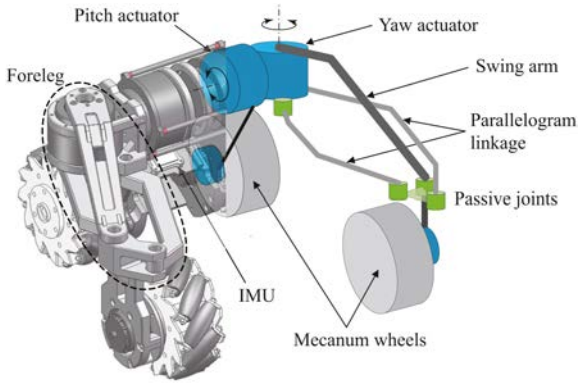

Fig. 1. Overview of the proposed robot design.

design enabled the robot to transform into different operational modes, vary its footprint for improving its trafficability, and carry objects with its forelegs for transportation purposes. The primary contributions of this study can be summarized as follows:

1) A novel design of a transformable mobile robot, capable of varying locomotion configurations and transporting objects using integrated mechanisms, is proposed;
2) The kinematics of Mecanum wheels with asymmetric arrangement variation are derived and examined;
3) The control and operation of the robot, including operating in different modes and switching between modes, are implemented and demonstrated.

The remainder of this paper is organized as follows. Section II presents the proposed design and feasible operational modes. Section III explains the kinematics and control of the different operational modes. The experiments performed to verify the proposed design and analysis are described in Section IV. Finally, Section V concludes the study.

II. System Overview

A. Design

Fig. 1 depicts the overview of the proposed robot design. The robot comprises four Mecanum wheels, two of which are attached to the chassis with the other two linked to the chassis via forelegs. Each foreleg includes a pitch joint and parallelogram linkage mechanism driven by the yaw joint. Therefore, the robot can extend or retract its forelegs by rotating the pitch joints or swing its forelegs forward and backward by rotating the yaw joints, similar to a mantis moving its two forelegs. The parallelism of the wheel axles is always ensured owing to the use of the parallelogram linkage mechanism. This configuration not only enables the robot to change its operational modes and vary its height and footprint but also provides transportation capabilities to the robot. Each Mecanum wheel was driven by a motor (M3508, DJI), and both the pitch and yaw joints were active (RMD-X6 S2, MyActuator). Therefore, the robot contained eight actuators. An inertial measurement unit (IMU; JY901S, WitMotion) was mounted on the chassis for motion control. Batteries and the STM32-based controller were integrated into the chassis such that the robot remained untethered. Table I summarizes the technical specifications of the proposed robot.

B. Operational Modes

Fig. 2 illustrates the three different operational modes of the robot achieved because of its unique configuration.

TABLE I
Specifications of the Proposed Robot

Size	Normal (Quadrilateral four-wheel mode) 314 mm × 304 mm × 305 mm
	Narrowest (Collinear four-wheel mode) 594 mm × 142 mm × 305 mm
	Lowest (Quadrilateral four-wheel mode) 314 mm × 347 mm × 185 mm
Weight	8.9 kg
Moving speed	0–2.5 m/s
Degrees of freedom	8 (2 per foreleg, 1 per wheel)
Angle limits of forelegs	Pitch: −18°–126° Yaw: 0°–90°

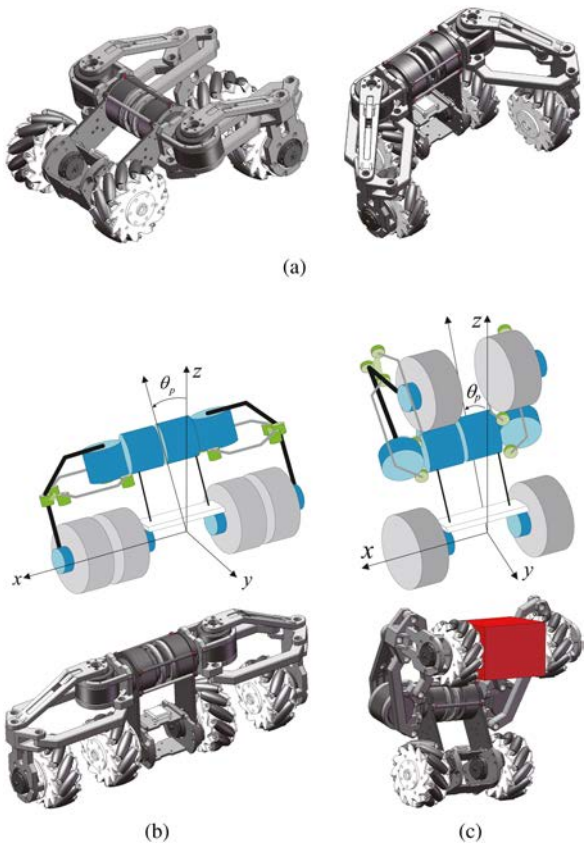

Fig. 2. Three operational modes. (a) Quadrilateral four-wheel mode. (b) Collinear four-wheel mode. (c) Upright two-wheel mode.

1) Quadrilateral Four-Wheel Mode: The footprint of the robot in this mode is quadrilateral, rendering the robot omnidirectional. The robot behaves as a normal Mecanum wheeled mobile platform with an asymmetric wheel arrangement when the forelegs remain stationary. However, the height and footprint of the robot vary because the relative positions of the four wheels can be changed by moving the forelegs. For instance, the robot can lower its height to pass through low-ceiling passageways if necessary (Fig. 3(a)). Additionally, the performance of the robot can be varied by changing its Mecanum wheel arrangement. Particularly, the Mecanum wheel arrangement can switch between Type-X (yaw angles are less than 90°) and Type-O (yaw angles are greater than 90°). As reported in [17], the Type-X arrangement exhibits better stiffness and dexterity to achieve a more precise and stable omnidirectional movement. Furthermore, the performance differs as to the size of footprints, even for identical Type-X or Type-O arrangement.

IEEE Robotics and Automation Letters (RA-L) paper, presented at ICRA 2024, Yokohama, Japan. Cite as RA-L paper.

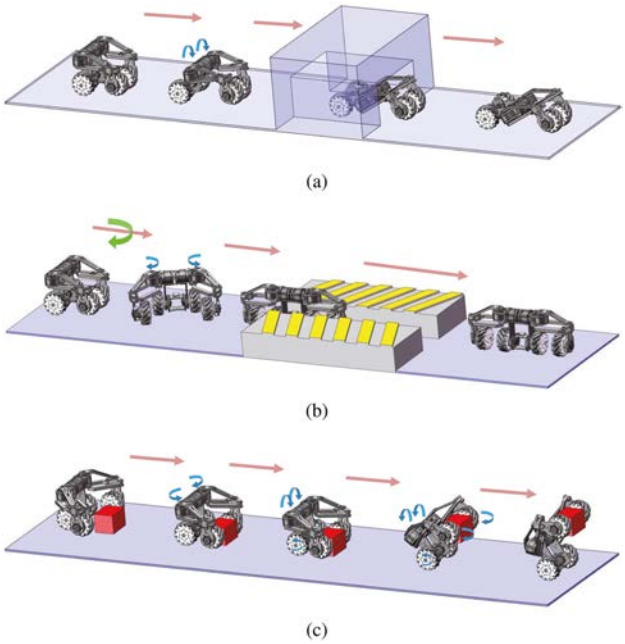

Fig. 3. Different operational modes for enhancing environmental adaptability. (a) Passing through low-ceiling passageways by lowering the posture. (b) Passing through narrow passages using the collinear four-wheel mode. (c) Transporting an object using the upright two-wheel mode.

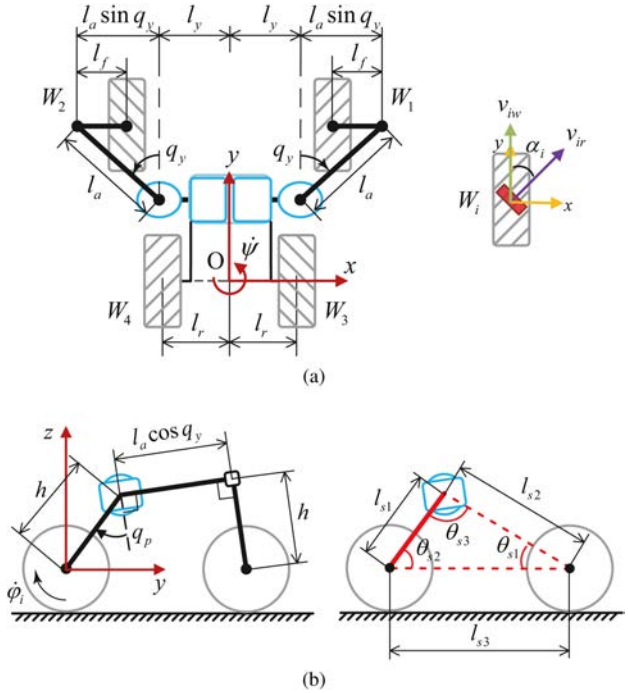

Fig. 4. Modeling of the robot in the quadrilateral four-wheel mode. (a) Top view. (b) Side View.

2) Collinear Four-Wheel Mode: The robot operates in this mode if its forelegs are retracted, with the yaw joints maintained constant at 90°. In this case, the four wheels are collinear and the robot minimizes its footprint, particularly its width. This allows the robot to pass laterally through narrow passages, as depicted in Fig. 3(b). According to [18], although the four Mecanum wheels are collinear, the robot can continue to move omnidirectionally. The robot in this mode is not statically balanced. Therefore, it must be considered as an inverted pendulum for dynamic balance control with an IMU in the loop.

3) Upright Two-Wheel Mode: As depicted in Fig. 3(c), the robot stands up and raises its two foreleg wheels in this mode, behaving as a wheeled inverted pendulum and maintaining the dynamic balance. The two forelegs serve as grippers, which can be opened and closed by rotating the yaw joints. With an appropriate dynamic balance control, the robot can pick up an object from the ground with its forelegs, stand up, and carry the object to its destination.

III. Kinematics and Control

Assuming that $\dot{\varphi}_i$ (i = 1, 2, 3, 4) denotes the angular velocity of the i-th Mecanum wheel and $\begin{bmatrix}\dot{x} & \dot{y} & \dot{\psi}\end{bmatrix}^{\mathrm{T}}$ represents the body velocity of the robot, we derived the kinematic relationship between $\dot{\varphi}_i$ and $\begin{bmatrix}\dot{x} & \dot{y} & \dot{\psi}\end{bmatrix}^{\mathrm{T}}$ in different modes.

A. Quadrilateral Four-Wheel Mode

Fig. 4 depicts the model of the robot operated in the quadrilateral four-wheel mode on a flat plane, where {O} denotes the body-attached frame, with O located on the rear wheel rotation axis in the center of the robot and the $\hat{z}$ axis always pointed vertically upwards. To simplify the control, the structures and motions of the left and right sides were assumed to be symmetrical. We introduced q_p and q_y to denote the rotation angles of the pitch and yaw joints on both sides, respectively.

The distances of the i-th Mecanum wheel relative to {O}, denoted as l_{ix} and l_{iy}, varied with the motion of the pitch and yaw joints. According to the geometric relationship shown in Fig. 4, the distances can be specifically represented as

$$\begin{bmatrix} l_{1x} & l_{1y} \\ l_{2x} & l_{2y} \\ l_{3x} & l_{3y} \\ l_{4x} & l_{4y} \end{bmatrix} = \begin{bmatrix} l_y + l_a \sin q_y - l_f & l_{s3} \\ l_y + l_a \sin q_y - l_f & l_{s3} \\ l_r & 0 \\ l_r & 0 \end{bmatrix}, \tag{1}$$

$$\begin{bmatrix} \dot{l}_{1x} & \dot{l}_{1y} \\ \dot{l}_{2x} & \dot{l}_{2y} \\ \dot{l}_{3x} & \dot{l}_{3y} \\ \dot{l}_{4x} & \dot{l}_{4y} \end{bmatrix} = \begin{bmatrix} (l_a \cos q_y)\dot{q}_y & \dot{l}_{s3} \\ (l_a \cos q_y)\dot{q}_y & \dot{l}_{s3} \\ 0 & 0 \\ 0 & 0 \end{bmatrix}, \tag{2}$$

where l_{s3} denotes the distance between the axles of the front and rear wheels. Fig. 4(b) indicates that the robot can be equivalent to a two segment mobile base. The equivalent parameters, such as l_{s1}, l_{s2}, and θ_{s3} are

$$\begin{bmatrix} l_{s1} \\ l_{s2} \\ \theta_{s3} \\ \dot{l}_{s1} \\ \dot{l}_{s2} \\ \dot{\theta}_{s3} \end{bmatrix} = \begin{bmatrix} h \\ \sqrt{h^2 + l_a^2 \cos^2 q_y} \\ q_p + \arctan((l_a \cos q_y)/h) \\ 0 \\ (-l_a^2 \dot{q}_y \sin q_y \cos q_y)/l_{s2} \\ \dot{q}_p - (l_a h \dot{q}_y \sin q_y)/l_{s2}^2 \end{bmatrix}, \tag{3}$$

where h and l_a represent the length of linkages indicated in Fig. 4. Applying law of cosines in trigonometry yields

$$\begin{bmatrix} l_{s3} \\ \dot{l}_{s3} \end{bmatrix} = \begin{bmatrix} \sqrt{l_{s1}^2 + l_{s2}^2 - 2l_{s1}l_{s2}\cos\theta_{s3}} \\ (l_{s2}\dot{l}_{s2} - l_{s1}\dot{l}_{s2}\cos\theta_{s3} + l_{s1}l_{s2}\dot{\theta}_{s3}\sin\theta_{s3})/l_{s3} \end{bmatrix}. \tag{4}$$

The velocity (v_{ix} and v_{iy}) of the i-th Mecanum wheel must satisfy the following kinematic constraint:

$$\begin{aligned} v_{ix} &= \sin\alpha_i v_{ir} \\ v_{iy} &= v_{iw} + \cos\alpha_i v_{ir} = R_w\dot{\varphi}_i + \cos\alpha_i v_{ir}, \end{aligned} \tag{5}$$

where v_{ir} and v_{iw} denote the angular velocities of the roller and wheel, α_i denotes the angle between the roller and wheel axes, and R_w represents the wheel radius. For the proposed robot, $\alpha_1 = \alpha_4 = 45°$ and $\alpha_2 = \alpha_3 = -45°$. Based on the assumption that no slippage occurs between the wheel and ground, the velocity of the i-th Mecanum wheel with respect to {O} can be calculated with the body velocity of the robot and motion of the forelegs, as

$$\begin{bmatrix} v_{1x} & v_{1y} \\ v_{2x} & v_{2y} \\ v_{3x} & v_{3y} \\ v_{4x} & v_{4y} \end{bmatrix} = \begin{bmatrix} \dot{x} - l_{1y}\dot{\psi} + \dot{l}_{1x} & \dot{y} + l_{1x}\dot{\psi} + \dot{l}_{1y} - R_w\dot{\theta}_{s1} \\ \dot{x} - l_{2y}\dot{\psi} - \dot{l}_{2x} & \dot{y} - l_{2x}\dot{\psi} + \dot{l}_{2y} - R_w\dot{\theta}_{s1} \\ \dot{x} - l_{3y}\dot{\psi} + \dot{l}_{3x} & \dot{y} + l_{3x}\dot{\psi} + \dot{l}_{3y} + R_w\dot{\theta}_{s2} \\ \dot{x} - l_{4y}\dot{\psi} - \dot{l}_{4x} & \dot{y} - l_{4x}\dot{\psi} + \dot{l}_{4y} + R_w\dot{\theta}_{s2} \end{bmatrix} \tag{6}$$

where θ_{s1} and θ_{s2} denote the two equivalent angles indicated in Fig. 4(b); $\dot{\theta}_{s1}$ and $\dot{\theta}_{s2}$ can be calculated based on (3) and (4). Combining (5) and (6) yields the inverse kinematics of the robot, as follows:

$$\begin{bmatrix} \dot{\varphi}_1 \\ \dot{\varphi}_2 \\ \dot{\varphi}_3 \\ \dot{\varphi}_4 \end{bmatrix} = \frac{\mathbf{M}}{R_w}\begin{bmatrix} \dot{x} \\ \dot{y} \\ \dot{\psi} \end{bmatrix} + \frac{1}{R_w}\begin{bmatrix} \dot{l}_{1y} - \dot{l}_{1x} \\ \dot{l}_{2y} - \dot{l}_{2x} \\ 0 \\ 0 \end{bmatrix} + \begin{bmatrix} -\dot{\theta}_{s1} \\ -\dot{\theta}_{s1} \\ \dot{\theta}_{s2} \\ \dot{\theta}_{s2} \end{bmatrix}, \tag{7}$$

where

$$\mathbf{M} = \begin{bmatrix} -1 & 1 & l_{1x} + l_{1y} \\ 1 & 1 & -l_{2x} - l_{2y} \\ 1 & 1 & l_{3x} \\ -1 & 1 & -l_{4x} \end{bmatrix}. \tag{8}$$

Note that the front and rear parts of the robot are asymmetric, which differs from the conventional Mecanum wheeled mobile robots. When $\dot{x} \neq 0$, the torque generated by the frictional forces is usually not zero. Consequently, the robot will turn slightly under the action of frictional torque. An additional angular velocity should be compensated to (7) to cancel the self-turning motion and ensure the robot move laterally as intended. The derivation of the additional angular velocity can be found in the appendix, with the form as

$$\dot{\psi}_e = A\dot{x}, \tag{9}$$

with

$$A = \frac{\eta m_r}{J(q_p, q_y)}, \tag{10}$$

where η is a linkage-related parameter that can be computed with (24), m_r refers to the mass of the robot, and $J(q_p, q_y)$ represents the rotational inertia around the instantaneous center of mass (CoM) described in {O} and can be approximately calculated with (22). Therefore, by subtracting Am_{i3} from m_{i1} (m_{ij} represents the elements of $\mathbf{M}$), (8) becomes

$$\mathbf{N} = \begin{bmatrix} -1 - A(l_{1x} + l_{1y}) & 1 & l_{1x} + l_{1y} \\ 1 + A(l_{2x} + l_{2y}) & 1 & -l_{2x} - l_{2y} \\ 1 - Al_{3x} & 1 & l_{3x} \\ -1 + Al_{4x} & 1 & -l_{4x} \end{bmatrix}. \tag{11}$$

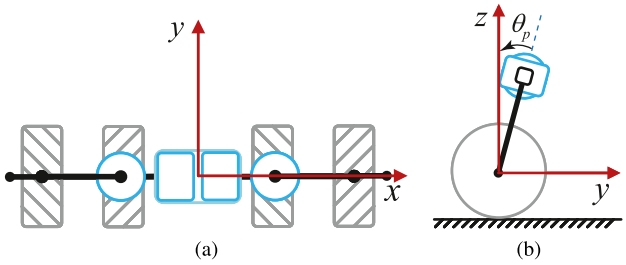

Fig. 5. Model of the robot in the collinear four-wheel mode. (a) Top view. (b) Side View.

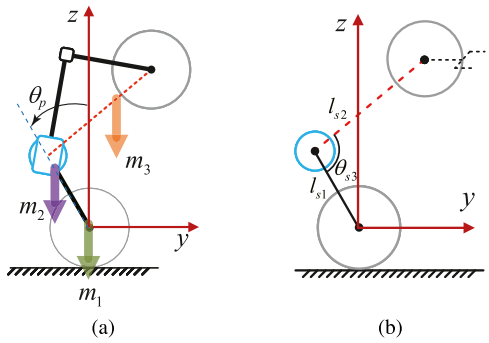

Fig. 6. Simplified model of the robot in the upright two-wheel mode. (a) Mass distribution. (b) Parameters.

B. Collinear Four-Wheel Mode

Fig. 5 depicts the model of the robot operating in the collinear four-wheel mode, which can be considered as a unique case of the quadrilateral four-wheel mode. Due to the frictional torque cannot be self-canceled, the compensation of additional angular velocity is also required. The velocity control of wheels in this mode should ensure both movement and balance of the robot. Therefore, we substituted $q_y = 90°$, $q_p = 0°$ and $\dot{q}_y = \dot{q}_p = 0$ in (7) and (11) and introduced θ_p to represent the tilt angle of the robot to yield the inverse kinematics of this mode, as follows:

$$\begin{bmatrix} \dot{\varphi}_1 \\ \dot{\varphi}_2 \\ \dot{\varphi}_3 \\ \dot{\varphi}_4 \end{bmatrix} = \frac{\mathbf{N}}{R_w}\begin{bmatrix} \dot{x} \\ \dot{y} \\ \dot{\psi} \end{bmatrix} + \begin{bmatrix} \dot{\theta}_p \\ \dot{\theta}_p \\ \dot{\theta}_p \\ \dot{\theta}_p \end{bmatrix}. \tag{12}$$

C. Upright Two-Wheel Mode

Fig. 6 illustrates a simplified model of the robot in the upright two-wheel mode. As the foreleg wheels are lifted, the robot is no longer omnidirectional and can not move laterally. The foreleg wheels can be used to adjust the pitch angle of the gripped object to maintain its initial orientation. The inverse

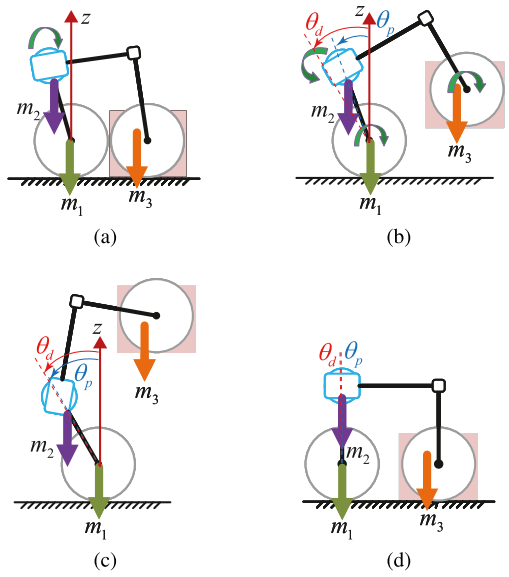

Fig. 7. Process of transporting an object. (a) Initial state; (b) lifting and (c) transporting the object; and (d) placing the down.

kinematics of the robot in this mode is

$$\begin{bmatrix}\dot{\varphi}_1\\ \dot{\varphi}_2\\ \dot{\varphi}_3\\ \dot{\varphi}_4\end{bmatrix} = \frac{1}{R_w}\begin{bmatrix}0 & 0\\ 0 & 0\\ 1 & l_{3x}\\ 1 & -l_{4x}\end{bmatrix}\begin{bmatrix}\dot{y}\\ \dot{\psi}\end{bmatrix} + \begin{bmatrix}\dot{\theta}_p + \dot{q}_p\\ \dot{\theta}_p + \dot{q}_p\\ \dot{\theta}_p - \dot{\theta}_d\\ \dot{\theta}_p - \dot{\theta}_d\end{bmatrix}, \tag{13}$$

where θ_d denotes the desired tilt angle of the robot when the system is in the static equilibrium condition. Assuming that the gravity moment around the rear wheel axis generated by the concentrated masses m_2 and m_3 is denoted as $[\tau_2 \quad \tau_3]^{\mathrm{T}}$, the static equilibrium equation can be obtained as

$$\tau_2 = \tau_3, \tag{14}$$

$$\begin{bmatrix}\tau_2\\ \tau_3\end{bmatrix} = \begin{bmatrix}(\varepsilon_2 l_{s1}\sin\theta_p)m_2\, g\\ (\varepsilon_3 l_{s2}\sin(\theta_p+\theta_q) - l_{s1}\sin\theta_p)m_3\, g\end{bmatrix}, \tag{15}$$

where ε_2 and ε_3 represent the correction coefficients that approximate the gravity lever considering the mass of linkages, which can be experimentally determined. As $\theta_d = \theta_p$ in the static equilibrium, substituting (15) into (14) yields

$$\theta_d = \arctan\frac{\varepsilon_3 l_{s2} m_3 \sin\theta_{s3}}{\varepsilon_2 l_{s1} m_2 + l_{s1} m_3 - \varepsilon_3 l_{s2} m_3 \cos\theta_{s3}}. \tag{16}$$

According to (3), because θ_{s3} and l_{s2} are functions of q_y and q_p, θ_d is neither a constant nor unique during the lift-up process.

Fig. 7 depicts the process of the robot transporting an object. First, the robot approaches the target object and grips it using the two foreleg wheels. An effective way to ease the lift-up motion and rapidly achieve a balanced state is to adjust m_3 to the rear wheel axis as close as possible, such that the gravity of the upper body contributes to the forelegs being raised to lift the object when the robot moves forward. However, to prevent the robot from self-interfering, the constraint $l_{s3} \geqslant 2R_w$ must be satisfied, resulting in

$$q_p^{\min} = \arccos(B) - \arctan((l_a\cos q_y)/h), \tag{17}$$

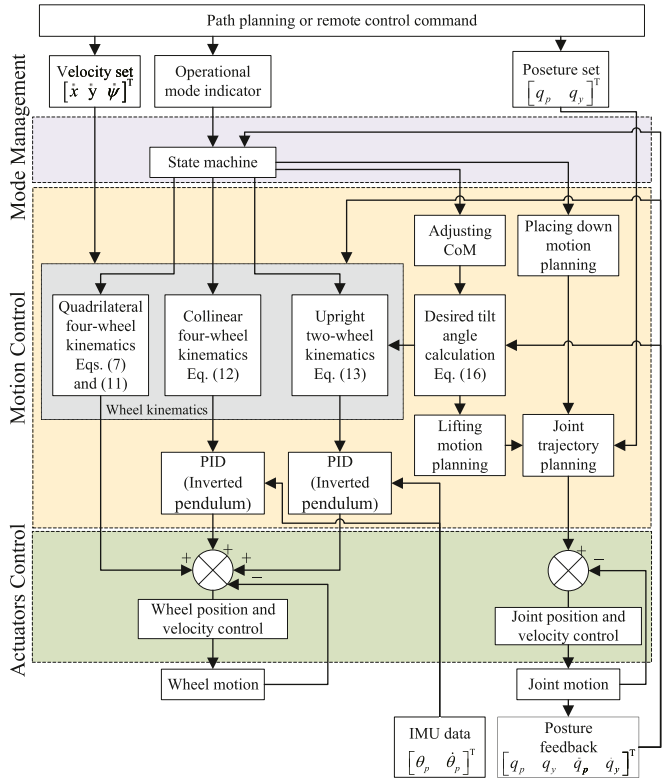

Fig. 8. Control architecture.

where

$$B = \frac{l_{s1}^2 + l_{s2}^2 - 4R_w^2}{2l_{s1}l_{s2}}.$$

Therefore, the robot should rotate the pitch joint to $q_p^{\min}$ to adjust its CoM and prepare for lifting its forelegs. The robot then lifts the object by coordinating the pitch joints and rear wheels. After lifting the object, the robot can be controlled using a proportional-integral-derivative (PID) controller to maintain balance according to (13). The robot begins to move and transports the object to its destination. Finally, the robot placed the object down and releases it.

D. Control Architecture

Fig. 8 illustrates the control architecture of the proposed robot. The robot accepts inputs, such as an operational mode indicator, a target posture and the moving velocity, either from path planning or remote control. A finite-state machine was used to manage the robot mode switching operations according to the operational mode indicator and posture feedback. Therefore, appropriate wheel kinematics were automatically identified for three basic operational modes by the posture feedback. Two PID controllers were implemented with the IMU data, to maintain balance in the collinear four-wheel and upright two-wheel modes. Joint motion was generated if the robot was commanded to switch to (out of) the upright two-wheel mode or change its footprint (height or gripper state) by directly sending the target posture. Accordingly, wheel motion caused by the joint movement was coordinately generated based on the posture feedback as it has been considered in the wheel kinematic model.

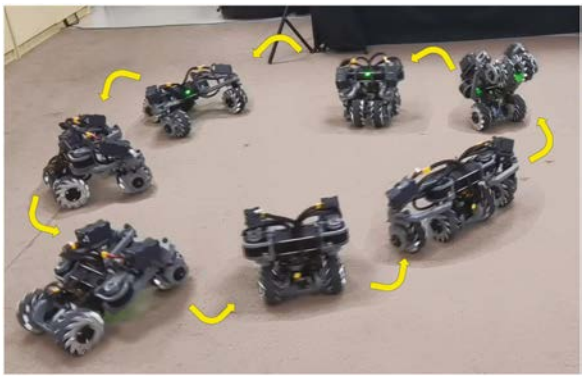

Fig. 9. Test on mode switching and basic motion control.

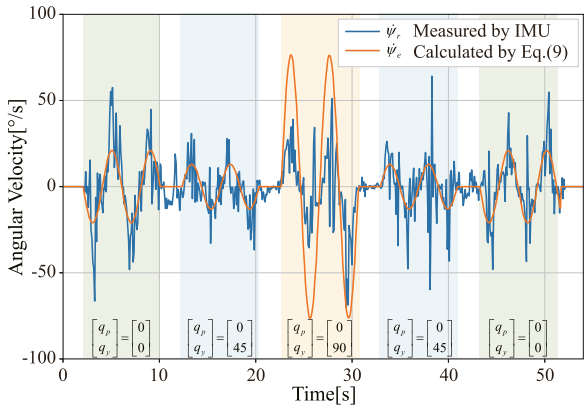

Fig. 10. Additional angular velocity measured by IMU and calculated using (9) when the robot is moving laterally.

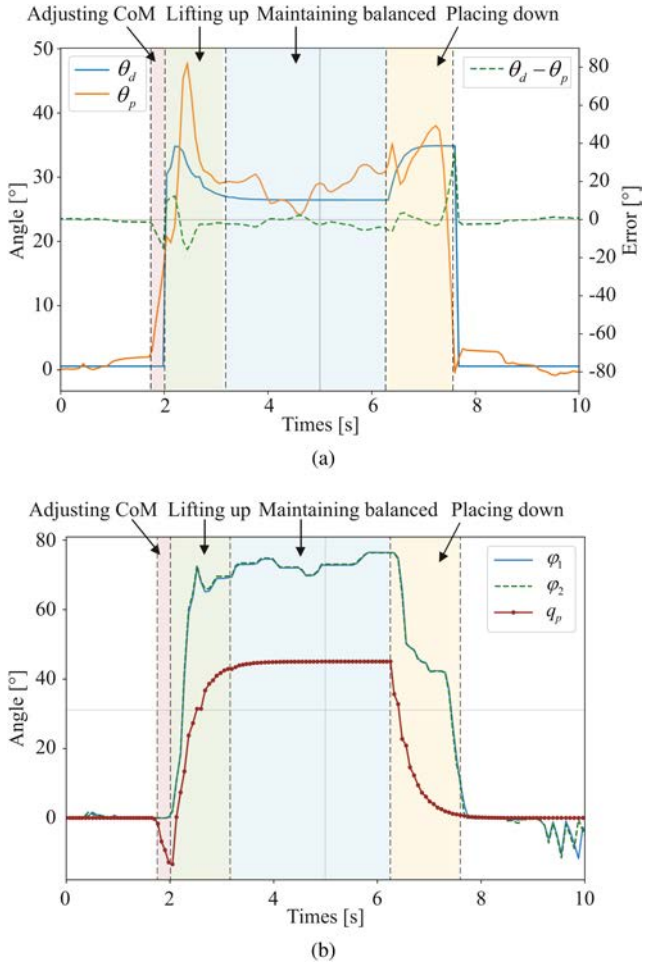

Fig. 11. Desired and measured tilt angles, foreleg wheel angles, and pitch joint angles during an object transportation process. (a) Plot of the desired and measured tilt angles and their errors. (b) Plot of the wheel and joint angles.

IV. Experiments

The effectiveness of the proposed design, kinematics and control were verified by performing three tests. A demonstration video of these three tests is provided in the supplementary material (a demonstration video) is mentioned at the footnotes on the first page of the paper, and can be downloaded on the paper's web page.

A. Verification of Mode Switching and Basic Motion Control

The first test was used to verify the robot kinematics derived in Section III. In the first half of the test, the robot was telecontrolled to move and vary the operational modes. Fig. 9 depicts the images extracted from the demonstration video. During the test, the robot exhibited the capability to smoothly complete a circular movement in three different operational modes in sequence. Furthermore, the robot successfully changed its height and footprint while moving in the quadrilateral four-wheel mode.

In the second half of the test, we measured the additional angular velocity in the quadrilateral and collinear four-wheel modes. The robot was instructed to move laterally with three different postures and a velocity of $\begin{bmatrix}\dot{x} & 0 & 0\end{bmatrix}^{\mathrm{T}}$, where $\dot{x} = 0.52\sin(\pi t/2)$. In this case, if the angular velocity measured by the IMU was not zero, it was considered to represent an additional component generated by the frictional torque. Fig. 10 presents the corresponding results. As indicated in the figure, the plot calculated using (9) reflects the additional angular velocity measured by the IMU, particularly in the quadrilateral four-wheel mode, which verifies the derived kinematics of the Mecanum wheels with asymmetric arrangements. The calculation accuracy of the CoM and rotational inertia dominates the magnitude of errors. A comparison of the robot movement with and without compensation was provided in the demonstration video, which affirmed the necessity of considering the additional angular velocity.

B. Evaluation of the Ability to Transport Objects

The second test evaluated the ability of the robot to transport objects without using any additional auxiliary devices. The robot was initially controlled to open its foreleg-wheel gripper and then close it to grip a red box with dimensions of 112 mm × 120 mm × 84 mm, which weighted 122.4 g. The box was placed down after transporting it for a short distance. Fig. 11(a) depicts the desired and measured tilt angles (θ_d and θ_p) and their errors observed during the entire transportation process. The mean error between θ_d and θ_p was approximately

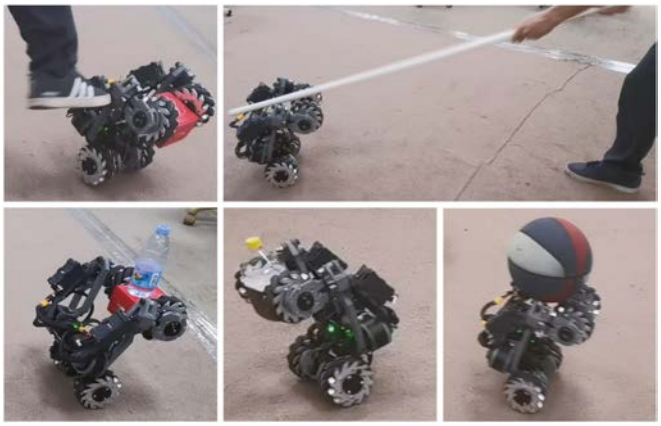

Fig. 12. Testing the ability of the robot to maintain the upright two-wheel mode.

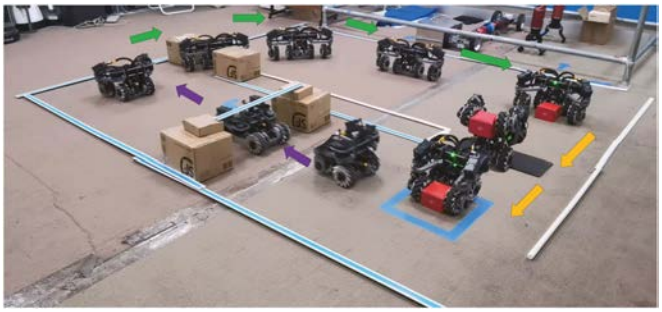

Fig. 13. Testing the applicability of the robot.

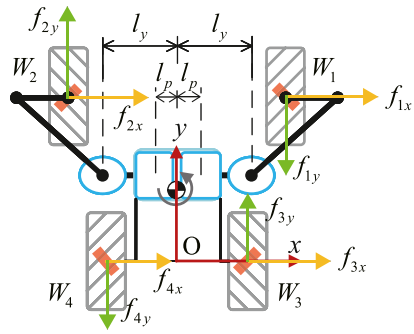

Fig. 14. Simplified model for deriving the additional angular velocity.

3.48°, which indicated that the actual tilt angle maintained its desired value under the proposed control. Consequently, the robot maintained its balance throughout the transportation. Fig. 11(b) plots the foreleg wheel angles (φ_1 and φ_2) required to maintain the top surface of the object horizontal and the pitch joint angles (q_p) corresponding to the four phases. As observed in the video and figure, the robot adjusted the CoM by reducing the pitch angles, which was beneficial for preparing for lifting. After that, the desired tilt angle was initialized. The lifting action was then achieved by rapidly increasing the pitch joint angles and moving forward coordinately, resulting in rapid decrease of the actual tilt angle. Once the object was lifted, the pitch joints could no longer move, and the desired tilt angle remained constant while the robot maintained its balance through the motion of the rear wheels.

Tests were also conducted to verify the ability of the robot to maintain the upright two-wheel mode under external disturbances, as presented in Fig. 12. In the tests, the robot demonstrated adequate robustness against external disturbances, such as kicking with legs, hitting with a stick, and unexpected changes in object weight, and successfully maintained the upright two-wheel mode.

C. Demonstration of the Applicability to Complex Missions

A third test was conducted to demonstrate the applicability of the proposed robot. Fig. 13 depicts the images extracted from the demonstration video. During the test, the robot sequentially and continuously passed through confined passages with restricted heights or widths, picked the target box, carried it, and passed through a raised barrier to reach the destination. This test demonstrated that the robot can be employed for complex missions that require transformation and object transportation.

V. Conclusion

In this study, we developed a novel transformable multi-mode leg-wheeled mobile robot. The unique configuration of the foreleg and Mecanum-wheels enabled the robot to exhibit three different operational modes and switch between any two modes without external assistance. The robot not only remained omnidirectional when operating in the quadrilateral or collinear four-wheel mode but varied its height and footprint to pass through confined spaces. Moreover, in the upright two-wheel mode, the robot was capable of utilizing its unique integrated foreleg-wheel mechanism to transport objects. The kinematics and control of the three operational modes were proposed and experimentally verified. We found that an additional angular velocity existed for the mobile robots with four Mecanum wheels, wherein the front and rear parts were asymmetrically arranged. The robot demonstrated favorable trafficability and object-transportation abilities.

In the future, we intend to study and improve the performance of the proposed robot when transporting objects and evaluate the control accuracy of complex motions considering multiple operational modes. Additionally, we plan to install appropriate external sensors for the robot to sense the local environment and autonomously switch to the appropriate operational mode.

Appendix

In this section, we derived the additional angular velocity caused by the frictional torque when $\dot{x} \neq 0$. Fig. 14 depicts a simplified model for analyzing the friction forces. For the i-th Mecanum wheel, its friction force maintain the following relationship:

$$f_{iy} = -\cot \alpha_i f_{ix}, \tag{18}$$

with $\alpha_1 = \alpha_4 = 45°$ and $\alpha_2 = \alpha_3 = -45°$ for the proposed robot. Considering the nonuniform mass distribution, the friction forces applied on the front and rear wheels satisfy

$$\begin{aligned} f_{3x} &= k f_{1x}, \quad f_{3y} = -k f_{1y} \\ f_{4x} &= -k f_{2x}, \quad f_{4y} = -k f_{2y}, \end{aligned} \tag{19}$$

TABLE II
TABLE OF PARAMETERS FOR THE PROTOTYPE

Parameter	Unit	Value	Parameter	Unit	Value
h	m	0.136	l_a	m	0.168
l_f	m	0.068	l_r	m	0.096
l_p	m	0.039	l_y	m	0.119
b_p	m	0.060	b_y	m	0.060
b_w	m	0.051	R_w	m	0.063
R_p	m	0.030	R_y	m	0.030
m_2	kg	2.344	m_3	kg	2.120
m_p	kg	0.586	m_y	kg	0.586
m_w	kg	1.060	m_r	kg	6.584

where $k = (l_{s3} - l_{cy})/l_{cy}$, and (l_{cx}, l_{cy}) is the center of mass described in $\{O\}$, as follows:

$$l_{cx} = 0$$
$$l_{cy} = \left[\sum m_{iw} l_{iy} + 2(m_p + m_y) l_{s1} \cos\theta_{s2}\right] / m_r, \quad (20)$$

where m_{iw}, m_p, and m_y denote the mass of wheel, pitch and yaw joints, respectively; $m_r = \sum m_{iw} + 2(m_p + m_y)$ considering that the four wheels, two pitch and two yaw joints contribute to more than 74% of the robot mass.

According to the Newton's law, the robot motion can be expressed as

$$\int \sum f_{ix} dt = m_r \dot{x}$$
$$\int [f_{1y} l_{1x} - f_{2y} l_{2x} + f_{3y} l_{3x} - f_{4y} l_{4x} - f_{1x}(l_{s3} - l_{cy}) - f_{2x}(l_{s3} - l_{cy}) + f_{3x} l_{cy} + f_{4x} l_{cy}]\, dt = J(q_p, q_y)\dot{\psi}_e, \quad (21)$$

where $J(q_p, q_y)$ represents the rotational inertia around the instantaneous center of mass; $\dot{\psi}_e$ represents the additional angular velocity caused by the asymmetric friction torque. $J(q_p, q_y)$ can be approximately calculated as follows:

$$J(q_p, q_y) = \sum J_{iw} + 2J_p + 2J_y, \quad (22)$$

with

$$J_{iw} = m_w \left(\frac{b_w^2}{12} + \frac{R_w^2}{4}\right) + m_w \left[l_{ix}^2 + (l_{cy} - l_{iy})^2\right]$$
$$J_p = m_p \left(\frac{b_p^2}{12} + \frac{R_p^2}{4}\right) + m_p \left[(l_{cy} - l_{s1}\cos\theta_{s2})^2 + l_p^2\right]$$
$$J_y = \frac{1}{2} m_y R_y^2 + m_y \left[(l_{cy} - l_{s1}\cos\theta_{s2})^2 + l_y^2\right],$$

where b_w, b_p, and b_y denote the height of cylindrical wheels, pitch and yaw joints, R_w, R_p and R_y represent their radii, and l_p and l_y are indicated in Fig. 14. Applying (18) and (19) to (21) and eliminating the friction force components yield

$$\dot{\psi}_e = \frac{\eta m_r}{J(q_p, q_y)} \dot{x}, \quad (23)$$

where

$$\eta = \frac{-l_{1x} - l_{2x} + k l_{3x} + k l_{4x} - 2(l_{s3} - l_{cy}) + 2k l_{cy}}{2(1+k)}. \quad (24)$$

Table II summarizes the parameters for the robot prototype.

REFERENCES

[1] H. Taheri and C. X. Zhao, "Omnidirectional mobile robots, mechanisms and navigation approaches," *Mech. Mach. Theory*, vol. 153, 2020, Art. no. 103958.

[2] S. Jiang et al., "Design, control and experiments of an agile omnidirectional mobile robot with active suspension," in *Proc. IEEE 18th Int. Conf. Autom. Sci. Eng.*, 2022, pp. 913–918.

[3] E. C. Orozco-Magdaleno, F. Gómez-Bravo, E. Castillo-Castañeda, and G. Carbone, "Evaluation of locomotion performances for a mecanum-wheeled hybrid hexapod robot," *IEEE/ASME Trans. Mech.*, vol. 26, no. 3, pp. 1657–1667, Jun. 2021.

[4] S. H. Yun, J. Park, J. Seo, and Y.-J. Kim, "Development of an agile omnidirectional mobile robot with GRF compensated wheel-leg mechanisms for human environments," *IEEE Robot. Autom. Lett.*, vol. 6, no. 4, pp. 8301–8308, Oct. 2021.

[5] F. Michaud et al., "Multi-modal locomotion robotic platform using leg-track-wheel articulations," *Auton. Robot.*, vol. 18, pp. 137–156, 2005.

[6] R. Cao, J. Gu, C. Yu, and A. Rosendo, "OmniWheg: An omnidirectional wheel-leg transformable robot," in *Proc. IEEE/RSJ Int. Conf. Intell. Robots Syst.*, 2022, pp. 5626–5631.

[7] W. Cheah et al., "MIRRAX: A reconfigurable robot for limited access environments," *IEEE Trans. Robot.*, vol. 39, no. 2, pp. 1341–1352, Apr. 2023.

[8] B. Gurol, M. Dal, S. M. Yesiloglu, and H. Temeltas, "Mechanical and electrical design of a four-wheel-drive, four-wheel-steer mobile manipulator with PA-10 arm," in *Proc. IEEE Int. Elect. Mach. Drives Conf.*, 2007, pp. 1777–1782.

[9] S. Zimmermann, R. Poranne, and S. Coros, "Go fetch! - Dynamic grasps using boston dynamics spot with external robotic arm," in *Proc. IEEE Int. Conf. Robot. Autom.*, 2021, pp. 4488–4494.

[10] A. Stentz et al., "CHIMP, The CMU highly intelligent mobile platform," *J. Field Robot.*, vol. 32, no. 2, pp. 209–228, 2015.

[11] M. Fuchs et al., "Rollin-Justin - Design considerations and realization of a mobile platform for a humanoid upper body," in *Proc. IEEE Int. Conf. Robot. Autom.*, 2009, pp. 4131–4137.

[12] N. Kashiri et al., "CENTAURO: A hybrid locomotion and high power resilient manipulation platform," *IEEE Robot. Autom. Lett.*, vol. 4, no. 2, pp. 1595–1602, Apr. 2019.

[13] Y. Gong et al., "Legged robots for object manipulation: A review," *Front. Mech. Eng.*, vol. 9, 2023, Art. no. 1142421.

[14] H. Deng et al., "Object carrying of hexapod robots with integrated mechanism of leg and arm," *Robot. Comput. Integr. Manuf.*, vol. 54, pp. 145–155, 2018.

[15] B. Leung, P. Billeschou, and P. Manoonpong, "Integrated modular neural control for versatile locomotion and object transportation of a dung beetle-like robot," *IEEE Trans. Cybern.*, early access, doi: 10.1109/TCYB.2023.3249467.

[16] E. Vollenweider, M. Bjelonic, V. Klemm, N. Rudin, J. Lee, and M. Hutter, "Advanced skills through multiple adversarial motion priors in reinforcement learning," in *Proc. IEEE Int. Conf. Robot. Autom.*, 2023, pp. 5120–5126.

[17] C. He et al., "Analysis of the mecanum wheel arrangement of an omnidirectional vehicle," *Proc. Inst. Mech. Eng., Part C: J. Mech. Eng. Sci.*, vol. 233, no. 15, 5329–5340, 2019.

[18] M. T. Watson, D. T. Gladwin, T. J. Prescott, and S. O. Conran, "Dual-mode model predictive control of an omnidirectional wheeled inverted pendulum," *IEEE/ASME Trans. Mech.*, vol. 24, no. 6, pp. 2964–2975, Dec. 2019.